AIAA JOURNAL
Vol. 41, No. 1, January 2003

Experimental Investigation of the Flow past a Submarine at Angle of Drift

David H. Bridges*
Mississippi State University, Mississippi State, Mississippi 39762
and
James N. Blanton,† Wesley H. Brewer,‡ and Joel T. Park§
U.S. Navy William B. Morgan Large Cavitation Channel, Memphis, Tennessee 38113-0428

When a submarine executes a high-speed turn, the sail experiences a crossflow velocity component, creating a vortex at the sail tip. The flowfield induced by the vortex creates higher pressures on the hull deck and lower pressures on the keel, leading to a nose-up pitching moment. Tests to examine such flows were conducted in the U.S. Navy's William B. Morgan Large Cavitation Channel in Memphis, Tennessee. A submarine model of 6.92-m length was tested at drift angles of 0, 5, and 9.5 deg, with the sail on and off, and at speeds up to 14.9 m/s. Pressure distributions and laser Doppler velocimeter surveys were obtained at two axial locations. Forces and moments were measured using an internal force balance. The pressure distributions were integrated to obtain section force coefficients, and the velocity data were used to estimate the vortex circulation. The pressure distributions were consistent with the hypothesized mechanism by which the vortex created the nose-up pitching moment. The pitching moment and sectional force coefficients demonstrated the nonlinear variations with drift angle predicted by theory. The circulation values were consistently somewhat higher than those obtained by other researchers.

Introduction

WHEN a submarine executes a high-speed turn, the sail of the submarine is placed at angle of attack. Because the sail in this condition is essentially a low-aspect-ratio, finite-span wing, a tip vortex is created that trails aft of the sail. This vortex modifies the pressure distribution on the rear of the submarine, causing a change in the pitching moment, which in turn causes a change in the direction of motion of the submarine in the vertical plane as well as the horizontal plane. The difficulties in submarine control that arise during such maneuvers are discussed by Gruner and Payne,[1] who describe the undesired forces and moments that are generated during a high-speed turn and who point out that manual control under these conditions is highly difficult, if not impossible. As discussed by Wright,[2] more accurate control of submarines during maneuvers became a more critical issue when more submarine missions began to be executed in shallow-water littoral regions.

The basic flow mechanisms at work in the submarine turning problem have been postulated for some time. They were summarized by Feldman[3] in terms of an inviscid flow model as follows: When the submarine is in a turning maneuver, there is a distribution of angle of drift developed along the length of the hull. The local angle of drift is relatively small along the forebody, but is relatively large along the afterbody. Lift is developed on the bridge fairwater due to the local angle of drift. It is assumed that there is a bound vortex at the quarter chord of the bridge fairwater and a tip vortex that trails aft. An image vortex is located inside the hull. This system of vorticity sets up circulation around the hull, which in combination with the local crossflow causes a hydrodynamic pressure difference to occur between the deck and keel. The normal force and pitching moment that result can be shown to vary with the angle of drift squared, at least for moderate angles of drift.[3]

In the experiments to be reported here, a submarine model was placed at a fixed angle of drift in a water tunnel facility, and pressures, forces, and velocities were measured. It was recognized that such an arrangement would not contain all of the flow features related to the submarine turn problem. The angle of drift at each point on the submarine would be the same, rather than the just described distribution discussed by Feldman.[3] Also, because this was in essence a "static" flowfield, the dynamics of the flow and the submarine response to the forces and moments generated would not be captured. The goal of these experiments was rather to obtain information about the magnitudes of pressure changes and vortex strengths that would be generated by the submarine at angle of drift and, in particular, to obtain these results at values of the Reynolds number much higher than previously studied and available in the open literature.

Previous Work on Submarines at Angle of Drift

To create an unclassified submarine geometry that could be used for both experimental and computational studies and, hence, provide data for validation of computational results, Groves et al.[4] designed and constructed an axisymmetric model, the Defense Advanced Research Projects Agency SUBOFF model. Roddy[5] tested the SUBOFF model in the David Taylor Model Basin (DTMB), measuring the forces and moments acting on the model for a range of configurations. The variations of pitching moment with drift angle demonstrate a nonlinear increase with angle of drift, as in the description by Feldman[3] given in the Introduction. Jonnalagadda[6] (also Jonnalagadda et al.[7] and Zierke[8]) computed the flow past the SUBOFF geometry using a Reynolds-averaged Navier–Stokes solver with a Baldwin–Lomax turbulence model. Jonnalagadda's results[6] are in general agreement with the pitching moment variations with angle of drift measured by Roddy[5] and also demonstrate the nonlinear variation of pitching moment observed in the experiments. Computational studies were also performed by Sung et al.[9] on the SUBOFF, DTMB Body 1, Albacore, and DTMB Model 4156 geometries undergoing constant-radius turns, and the results were compared with experiments. At zero pitch angle, the pitching moment exhibits a large negative value at zero yaw and a large positive value at 12-deg yaw, for both the experimental and computational studies considered. Sung et al. do not explain why the large negative value occurred at zero pitch and zero yaw.

Received 24 September 2001; revision received 17 August 2002; accepted for publication 18 August 2002.

*Associate Professor, Department of Aerospace Engineering, P.O. Drawer A. Senior Member AIAA.
†Engineer; currently Instrumentation Engineer, Flight Loads Laboratory, Mail Stop 2708, P.O. Box 273, NASA Dryden Flight Research Center, Edwards, CA 93523-0273.
‡Engineer; currently Graduate Student, Department of Aerospace Engineering, Mississippi State University, Mississippi State, MS 39762.
§Chief Engineer, P.O. Box 13428.

Particle displacement velocimetry (PDV) measurements were made of the flow around a submarine model in the DTMB rotating arm facility by Liu and Fu.[10] The model used was DTMB Model 5484 (described by Liu et al.[11]). The model was towed at a nominal speed of 2.57 m/s and at various pitch and yaw angles. Liu and Fu[10] report, among other things, the circulations measured in the vortex wake of the submarine and theoretical predictions based on the angle of attack of the sail. Liu and Fu also report measurements of the sail vortex trajectory downstream of the sail. These results will be compared with the current observations.

Wetzel et al.[12] (also Wetzel and Simpson[13]) investigated the effects of fins and jets in preventing or delaying crossflow separation on a model of a 688 Los Angeles-class submarine. The model was tested with sail but no stern appendages. Forces and moments were measured over a range of angles of drift. Various fin and jet configurations were studied to see which would prevent or delay crossflow separation. For the no-fin, no-jet case, the variation of pitching moment with drift angle repeated the nonlinear variation observed by others. The results with the vortex generators indicated that in general more attached flow caused an increase in the magnitude of the pitching moment coefficient for nonzero drift angles. The effects of the vortex shed by the sail were not directly addressed because no off-body flowfield measurements were reported.

Experimental Apparatus and Procedure

Facility

The current experiments were all conducted in the William B. Morgan Large Cavitation Channel (LCC),[14,15] located in Memphis, Tennessee. This facility is part of the Carderock Division of the Naval Surface Warfare Center (NSWCCD). The LCC has a test section that is 3.05 m high, 3.05 m wide, and 12.2 m long. The maximum test section speed is approximately 18 m/s, and the pressurization range for the test section extends from 3.5 to 415 kPa. The reported freestream turbulence level is less than 0.5%.

Model

The model used in the current experiments was a standard axisymmetric hull with a sail and four standard cruciform stern appendages. The hull length L was 6.92 m, and the diameter D was 0.623 m. The hull outline is shown in Fig. 1. The sail was 0.565 m long and 0.321 m high (Fig. 2). The aspect ratio of the sail, computed using the sail height as the "span," was 0.57. The sail had an airfoil cross section with a maximum thickness of 0.108 m, yielding a thickness ratio of 0.2. The leading edge of the sail was located 1.24 m from the nose, or $x/L = 0.18$. The model was suspended from the ceiling of the test section using a standard LCC strut arrangement with the pivot point located at $x/L = 0.22$. The hull could be mounted on the strut at various angles of attack. The sail was mounted on the side of the hull so that the flow past a submarine at angle of drift could be simulated. When the appropriate force and moment outputs of the force balance at a condition of zero angle of drift and zero velocity were used, the longitudinal location of the center of gravity of the submerged model was estimated as $x_{cg}/L = 0.32$. This model was designed for static tests and was not dynamically balanced to match the prototype, and so there was no known correlation between the center of gravity location of the model and prototype. Pressure taps were mounted in circumferential rings located at $x/L = 0.47$ and 0.65. The taps were 0.318 cm in diameter and spaced 10 deg apart in the circumferential direction, for a total of 36 taps at each axial location. With the definition of θ shown in Fig. 3, the region 0 deg $< \theta <$ 180 deg corresponds to the "deck" or "top" of the submarine hull, and the region 180 deg $< \theta <$ 360 deg corresponds to the "keel" or "bottom" of the submarine hull.

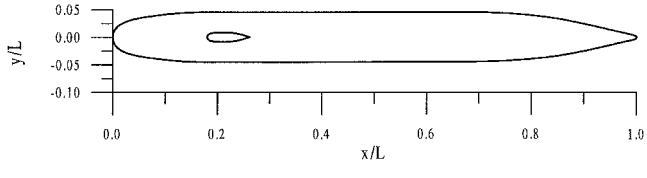

Fig. 1 Submarine model hull geometry (top view).

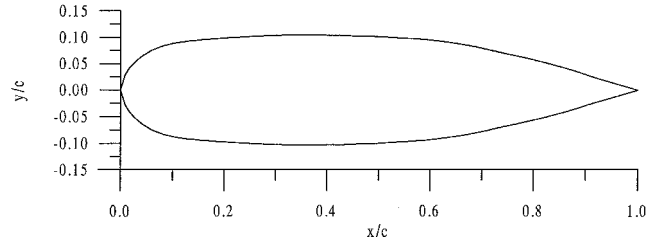

Foil section

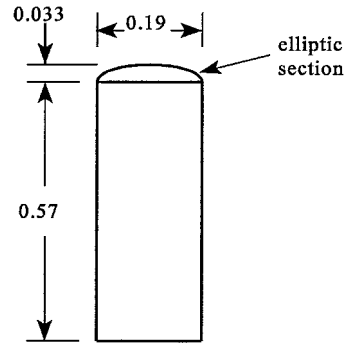

Front view (not to scale, dimensions in fractions of sail chord length *c*)

Fig. 2 Sail geometry.

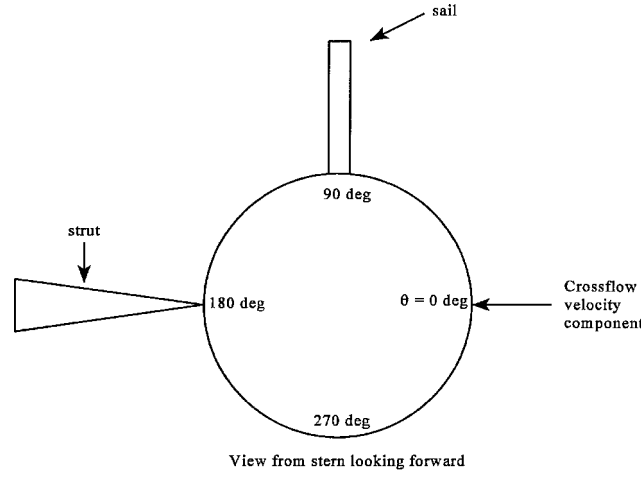

Fig. 3 Coordinate system orientation diagram.

Instrumentation

The velocity field was measured using a two-component Dantec® laser Doppler velocimeter (LDV) system.[16,17] The velocity components were measured in a reference frame fixed to the LCC test section. The axial or streamwise flow component u corresponded to the freestream velocity direction in the LCC, and the transverse or the vertical component w was in the direction perpendicular to the floor of the LCC test section. The pressures in the first test phase were measured using a Viatran Model 223 pressure transducer with a range of ±68.9-kPa differential and an accuracy of 0.25% of full scale, as stated by the manufacturer. For the second test phase, the transducer was replaced by a Viatran Model 274 transducer with a range of ±34.5 kPa and an uncertainty of 0.15% full scale, as stated by the manufacturer. The forces on the model were measured using an AMTI six-component internal force balance that was attached between the strut and the model. The reference point for all moment measurements was at the balance center, which was located at $x/L = 0.271$.

Effects of Blockage

The solid blockage of the test section varied from a minimum of approximately 3.5% with the model in the zero-drift, no-sail configuration to a maximum of approximately 8% for the model at maximum drift angle of 9.5 deg with the sail attached. The presence

of the model in the LCC test section created a pressure variation along the model due to this solid blockage. To remove as much of this effect from the pressure distributions as possible, the reference pressure in the definition of the pressure coefficient was taken as the circumferential average of the pressures measured on the hull at zero angle of drift with no sail. This value, denoted by $p_{\beta=0}$, was different for the two axial locations. Also, the reference velocity U used in the definition of the pressure coefficient was taken as the value measured in the LDV surveys halfway between the wall and the model, at the axial location of the pressure tap rings. When these "local freestream" values were used, which would be analogous to the local freestream or "edge" reference values for a boundary layer in a nonzero pressure gradient, the contribution from the blockage was reduced, and the effects of adding a sail and, thus, creating a tip vortex were emphasized. The blockage was only increased by a maximum of 0.8% when the sail was added, and because the changes in flow variables with the addition of the sail were of primary interest, no other blockage corrections were deemed necessary.

Uncertainty Analysis

Three variables were of primary interest in these experiments: pressures on the surface of the model, velocities in the flowfield away from the model, and forces acting on the model. A detailed uncertainty analysis of pressure measurements in the LCC was performed by Blanton[18] using the techniques outlined by Coleman and Steele.[19,20] A separate analysis of the uncertainty in LDV velocity measurements was performed by Blanton and Etter[17] using the same techniques.

The density was measured using the measured temperature of the water and a curve fit to calibration data obtained by measuring density as a function of temperature.[18] The total uncertainty in the density was estimated to be 0.0011 g/cm^3. The pressure coefficient was computed from

$$C_p(\theta) = \frac{p(\theta) - p_{\beta=0}}{\frac{1}{2}\rho U^2} \tag{1}$$

where $p(\theta)$ is the pressure at a particular model pressure tap and the other values are as defined earlier. The uncertainty in the value of the pressure coefficient was estimated using the techniques outlined by Coleman and Steele.[20] The primary source of systematic uncertainty in the pressure measurements was the uncertainty associated with the regression that was used to compute the pressure from the voltage output of the transducer. The sample standard deviations, from which the random uncertainties were obtained, tended to scale with the square of the velocity. The systematic uncertainty associated with the regression, on the other hand, was a fixed quantity. At lower speeds, this uncertainty tended to dominate the total uncertainty value. For more details concerning the uncertainty analysis, see the report by Bridges.[21]

Because the LDV system that was used to measure the velocities in the flowfield was essentially the same as that discussed by Blanton and Etter,[17] their result of 0.96% uncertainty in the velocity may be used directly here. The stated accuracy of the LDV traverse system was 0.05 mm.

The systematic uncertainty of the force balance was estimated to be 26.7 N in lift, or 0.12% of full scale, and 40.7 Nm in yaw, also 0.12% of full scale. The model had a flat base behind the rear fins. Because of the unsteadiness in the flow created by the wake of this flat base, the random uncertainty in the force and moment measurements tended to be somewhat large. The standard deviation of the pitching moment averaged over 1000 readings was generally 10% of the mean value. An estimate of 0.32 cm was used as the uncertainty in model length.

Test Grid

Tables 1, 2 and 3 record the conditions during each pressure measurement, LDV velocity survey, and force measurement, respectively. In addition to the model configuration for each test, Table 1 records the freestream speed in meters per second as measured by the LDV system. The last two columns of Table 1 show the Reynolds number Re_L based on the overall length L of 6.92 m and the freestream speed U and the crossflow Reynolds number Re_c based on the component of the freestream perpendicular to the axis of the model, $U \sin\beta$, and the diameter D of 0.623 m. The LDV velocity measurements were made on a grid of points perpendicular to the axis of the model and, thus, inclined to the freestream flow direction at the angle of drift being studied. The grids typically extended $0.5R$ to either side of the model and $0.5R$ above the sail, where R is the model radius (0.312 m). The grid spacing was typically $0.1R$, yielding a grid with 500–600 points. Additionally, grids with a finer resolution, using a grid spacing of $0.05R$, were used to obtained detailed mappings of the flow in the vicinity of the vortex core. The axial location of each velocity survey, the velocity component measured, and the type of grid used are included in Table 2. In Table 3, the values of the Reynolds number were computed using the LCC reference LDV velocity instead of the local freestream velocity.

For convenience, each test condition has been assigned a label listed in the first column of each table. The label for each phase 1 test condition begins with an A and the identifier for each phase 2 condition begins with a B. During the first phase, a support strut connected one of the rear fins of the model to the LCC test section wall, to stabilize the model. To isolate the effects of the tip vortex and remove the influence of the main strut as much as possible, the model was tested with the sail attached (sail on) and without the sail (sail off). Because forces were to be measured in the second phase, the support strut at the rear of the model had to be removed. Because of concerns about the resulting stability of the model, the maximum flow speeds during phase 2 were limited to nominally 9.3 m/s at 5 deg drift and 5.1 m/s at 9.5 deg drift.

Table 1 Test conditions for pressure measurements

Test	Sail	Drift angle, deg	LDV U, m/s	$Re_L \times 10e{-}6$	$Re_c \times 10e{-}6$
AP1	On	9.5	14.76	112.5	1.67
AP2	On	9.5	7.64	59.4	0.88
AP5	Off	9.5	14.76	124.9	1.86
AP7	Off	0	14.9	131.4	0
BP1	On	5	9.18	72.6	0.57
BP2	On	9.5	5.14	41.9	0.62
BP3	Off	5	9.18	75.4	0.59
BP4	Off	9.5	5.15	42.4	0.63
BP5	Off	0	10.5	87.0	0
BP6	Off	0	5.25	43.5	0

Table 2 Test conditions for velocity measurements

Test	Sail	Drift, deg	Traverse (x/L)	Velocity component	LDV grid	LDV U, m/s
AV01	On	9.5	0.47	u	Coarse	14.76
AV03	On	9.5	0.47	w	Coarse	7.64
AV04	On	9.5	0.47	w	Coarse	14.85
AV05	On	9.5	0.47	w	Fine	14.85
AV08	On	9.5	0.65	w	Coarse	14.85
BV02	On	5	0.47	w	Coarse	9.29
BV04	On	5	0.47	w	Fine	9.39
BV06	On	5	0.59	w	Fine	9.39
BV08	On	9.5	0.48	w	Coarse	5.23
BV10	On	9.5	0.48	w	Fine	5.24
BV14	On	9.5	0.62	w	Fine	5.28

Table 3 Test conditions for force measurements

Test	Sail	Drift, deg	Reference LDV U, m/s	$Re_L \times 10e{-}6$	$Re_c \times 10e{-}6$
BF1	On	5	9.172	72.5	0.569
BF2	On	9.5	5.142	41.9	0.623
BF3	On	9.5	5.139	41.8	0.621
BF4	Off	5	9.178	75.0	0.589
BF5	Off	5	9.178	75.6	0.594
BF6	Off	9.5	5.147	42.5	0.631
BF7	Off	0	10.28	85.1	0
BF8	Off	0	5.146	42.7	0

Results

Pressure Measurements

The pressure distributions obtained in this investigation were perhaps the most important results because they would provide evidence that would help confirm the postulated mechanisms for the creation of the pitching moment. Figure 4 shows the pressure coefficient distributions at the two different axial locations for the model at 9.5-deg drift and with the sail attached. It is obvious in Fig. 4 that the pressures are higher on the deck than they are on the keel. This would create a net down force on the hull aft of the sail and generally aft of the center of gravity of the submarine, contributing to a positive or nose-up pitching moment. The creation of a positive pitching moment is consistent with the results of Sung et al.[9] that show a change from a negative moment to a positive moment when the yaw angle in their study was increased from zero. Figure 5 shows the progression of pressure distributions at $x/L = 0.47$ as the configuration is changed. In Fig. 5, the uncertainty bars have been omitted for clarity. The first distribution is for the submarine at zero drift and with no sail attached, which is essentially an axisymmetric configuration (except for the strut) with respect to the oncoming flow. The second distribution is for $\beta = 9.5$ deg but with no sail attached. Here the distribution is what one would expect for the flow

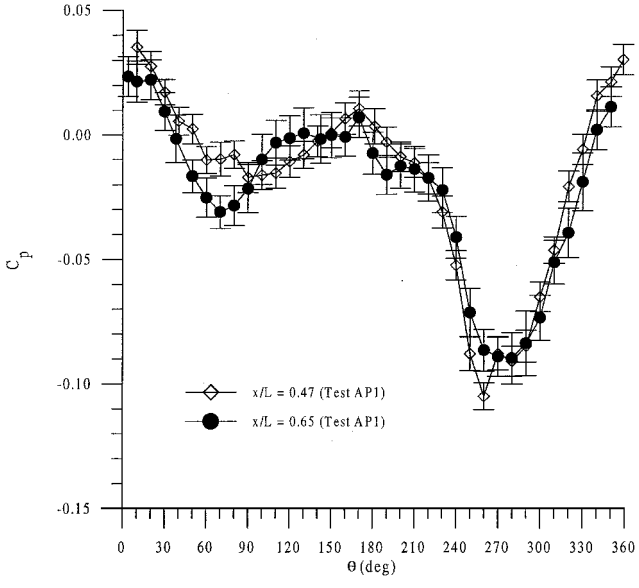

Fig. 4 Circumferential pressure distributions: β = 9.5 deg, U = 14.8 m/s, and sail on.

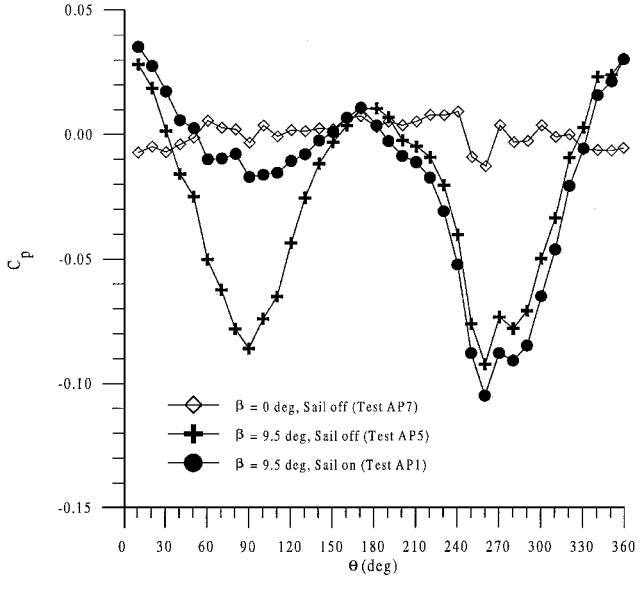

Fig. 5 Demonstration of the effect on pressures of adding the sail: x/L = 0.47.

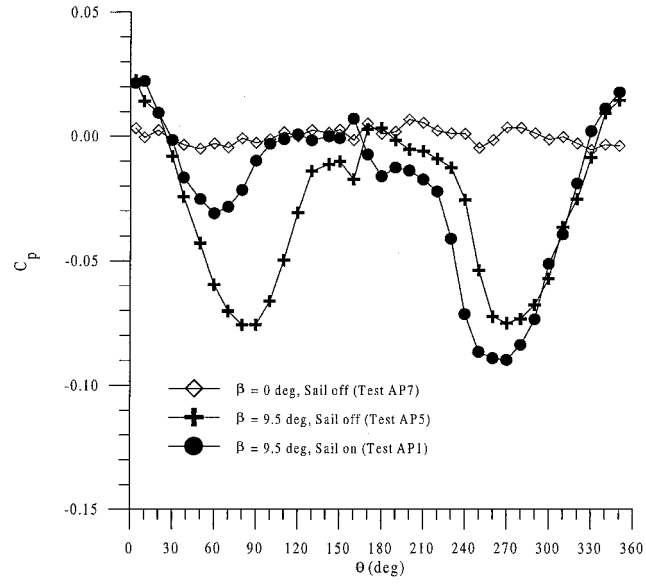

Fig. 6 Demonstration of the effect on pressures of adding the sail: x/L = 0.65.

past an inclined cylinder, with two suction peaks on the sides of the model corresponding to the regions of maximum flow acceleration. The third distribution repeats the pressures shown in Fig. 4, for the same angle of drift but with the sail attached. It is clear in comparing the second and third distributions that the addition of the sail has caused an increase in the pressures on the deck and a decrease in the pressures on the keel. The same progression of pressure distributions at the same drift angle is shown in Fig. 6 for $x/L = 0.65$. These pressure distributions also demonstrate the increase in pressure on the deck of the submarine and the decrease in pressure on the keel, again contributing to a net down force on the rear of the hull and a corresponding nose-up pitching moment.

Note that, in these pressure distributions, lower pressures occur on the side of the submarine opposite to the sail tip vortex and higher pressures on the side adjacent to the tip vortex. This may seem incorrect, particularly if one is thinking of the classic potential flow solution for a vortex in the presence of a circular cylinder, where the suction peak occurs at the point on the cylinder nearest the vortex. However, note that in the image vortex system for that solution the net circulation contained in a contour enclosing the cylinder is zero. That is not the case in the current experiments, in which it is assumed that there is finite circulation around the hull of the submarine. In this case, the situation is more analogous to the potential flow model of a rotating cylinder, in which a vortex is placed at the center of the cylinder. The resulting imbalance in pressures leads to the side force known as the Magnus force. If the submarine flowfield is considered in a crossflow plane, then it becomes apparent that the lower pressures should occur on the side away from the sail tip vortex.

The effects of Reynolds number on the pressure distributions are illustrated by Fig. 7, which demonstrates that, over the range of Reynolds number Re_L studied, there were very few Reynolds number Re_L effects. Where the Reynolds number effect was most obvious was in the region $240 < \theta < 310$ deg, which encompasses the keel of the submarine. In this region, the flow is attached to the model. It is postulated that at the higher values of Reynolds number Re_L, the boundary layer was thinner and the flow conformed more to the contour of the hull, pushing the pressure distribution more toward the corresponding inviscid flow distribution.

To remove the effects of the strut as much as possible, it was decided to examine the changes in the flow variables produced when the sail was added to the model at angle of drift. Figure 8 illustrates these changes. Figure 8 shows the quantity $\Delta C_p(\theta)$ defined as

$$\Delta C_p(\theta) = C_{p,\text{sail}}(\theta) - C_{n,\text{no sail}}(\theta) \tag{2}$$

or the pressure coefficient at a particular point when the sail is attached minus the pressure coefficient at the same point with no sail

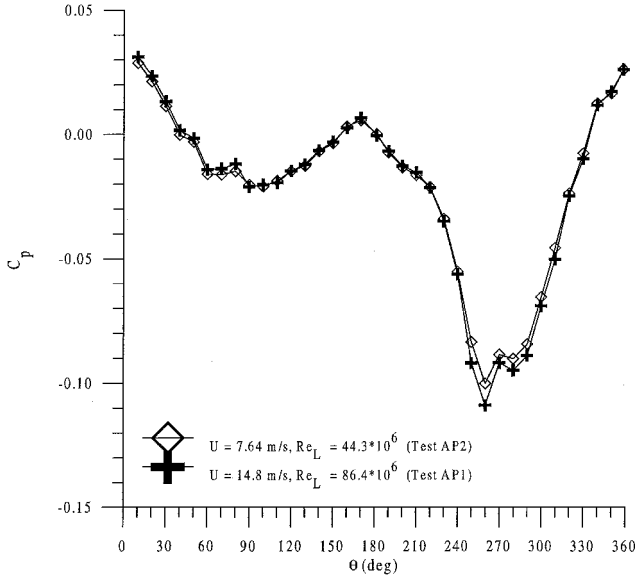

Fig. 7 Reynolds number effects: $\beta = 9.5$ deg, sail on, and $x/L = 0.47$.

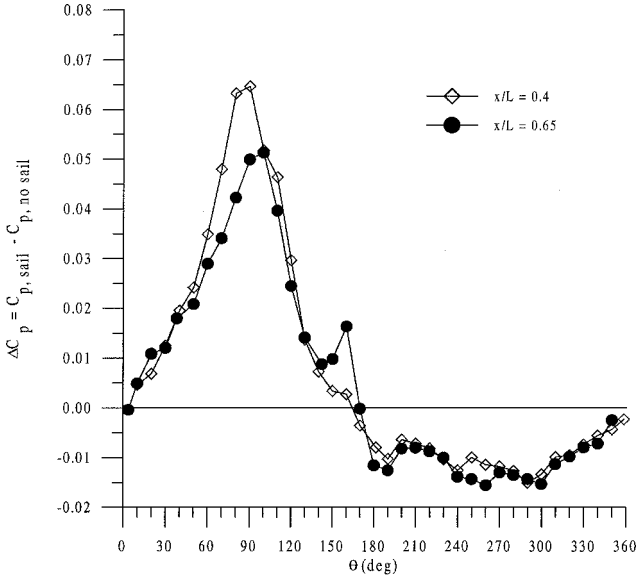

Fig. 8 Comparison of sail addition effects on pressure differences: $\beta = 9.5$ deg.

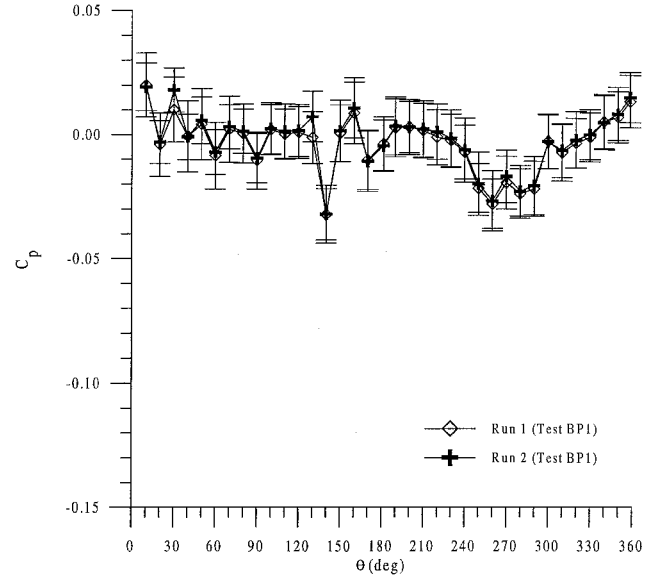

Fig. 9 Circumferential pressure distributions: $\beta = 5$ deg, $U = 9.18$ m/s, sail on, and $x/L = 0.47$.

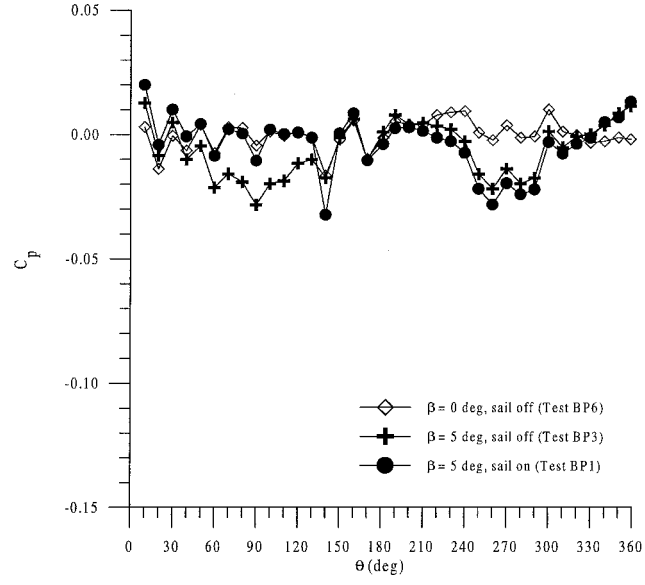

Fig. 10 Demonstration of the effect on pressures of adding the sail for $\beta = 5$ deg: $x/L = 0.47$.

attached. Figure 8 demonstrates, further, the increase of pressure on the deck of the submarine and the decrease on the keel for both axial locations at which pressures were measured. Figure 8 also illustrates the development of the pressure asymmetry with increasing axial distance. The magnitude seems to decrease slightly, and the peak in the positive pressure moves slightly in the circumferential direction. The shift in peak could be due to the change in circumferential location of the tip vortex relative to the submarine, so that the peak is attempting to "track" the tip vortex. Other than that shift and some peculiarities of the downstream distribution in the vicinity of $\theta = 180$ deg, the two $\Delta C_p(\theta)$ distributions are rather similar.

Figure 9 shows the pressure distributions obtained at $\beta = 5$ deg with the sail on. The uncertainty bars are somewhat larger than those in Fig. 4. The 5-deg drift measurements were made during the second phase of tests. The removal of the rear stabilization strut limited the top speed at which measurements could be made to $U = 9.18$ m/s. As explained earlier, the relatively large, fixed value of the systematic uncertainty from the regression used to compute the pressures from the transducer voltages meant that the uncertainty in C_p was essentially inversely proportional to the square of the velocity. For this reason, multiple runs were made at certain conditions to check the repeatability of the measurements. Two of these runs are included in Fig. 9, and they do show that the pressure distributions were repeatable.

Although it is somewhat difficult to make out in Fig. 9, the pressures on the deck of the hull are higher than the pressures on the keel. Note that an angle of drift of $\beta = 5$ deg is not large, and that the resulting crossflow velocity component is superimposed on a relatively large axial flow component. The pressure distributions at $\beta = 5$ deg were generally less organized than the distributions at $\beta = 9.5$ deg. The progression of pressure distributions is shown in Fig. 10, starting with $\beta = 0$ deg with no sail, then increasing β to 5 deg, but still with no sail, and then adding the sail at $\beta = 5$ deg. Once again it may be seen that the pressures on the deck go up and the pressures on the keel go down. The corresponding ΔC_p distributions, as defined by Eq. (2), are shown in Fig. 11 for both axial locations. The gap in the values at $x/L = 0.65$ is due to the necessity of removing pressure leads to make room in the strut for the force balance electrical cables in the second test phase.

The $\Delta C_p(\theta)$ distributions may be integrated to yield estimates of the change in the local vertical force coefficient per unit

Table 4 Sectional side force coefficients from pressure integrations

β, deg	Nominal U, m/s	x/L	Δc_z
5	9.18	0.47	0.0321
9.5	5.15	0.47	0.0877
9.5	7.64	0.47	0.0877
9.5	7.64	0.65	0.0805
9.5	14.8	0.47	0.0956
9.5	14.8	0.65	0.0895

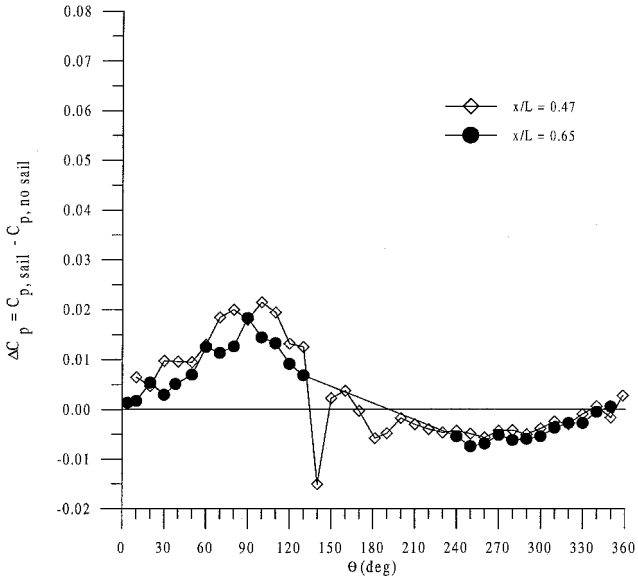

Fig. 11 Pressure difference due to addition of sail: $\beta = 5$ deg.

length. With the coefficient of change in vertical force Δc_z defined as

$$\Delta c_z = \Delta F_z \Big/ \tfrac{1}{2}\rho U^2 R \tag{3}$$

where ΔF_z is the change in vertical force per unit length when the sail is added and $R = D/2$ is the radius of the submarine, the exact integral

$$\Delta c_z = \int_0^{2\pi} \Delta C_p(\theta) \sin\theta \, d\theta \tag{4}$$

was estimated numerically for the $\Delta C_p(\theta)$ distributions in Figs. 8 and 11, yielding the values listed in Table 4. Because of the omitted pressure taps, the distributions for $\beta = 5$ deg and $x/L = 0.65$ were not integrated. The results indicate a nonlinear increase in the sectional side force coefficient with drift angle, as was expected. To illustrate this point further, Fig. 12 shows the development of the pressure differences with increasing drift angle that leads to the nonlinear variation of the sectional side force coefficient. The values of Δc_z in Table 4 are consistent in that the magnitude of the change in force coefficient generally increases with increasing Reynolds number, again perhaps due to the effects of a thinner boundary layer discussed earlier. They are also consistent in that the values at the downstream location are smaller than those at the upstream location, reflecting the decrease in magnitude of the pressure differences demonstrated in Figs. 8 and 11.

Force Measurements

The results for the pitching moment and vertical force coefficients are shown in Figs. 13 and 14. All moment results shown here are with reference to the force balance center, located at $x/L = 0.271$. No forces were measured on the model for zero drift angle and the sail-on configuration. As before, because these forces had to be measured on a model suspended by a large strut, the main quantity of interest in Figs. 13 and 14 is the difference between the sail-off and sail-on values. Both of these coefficients demonstrate the nonlinear variation expected from the analyses discussed earlier. The vertical force coefficient demonstrates the net down force that the submarine

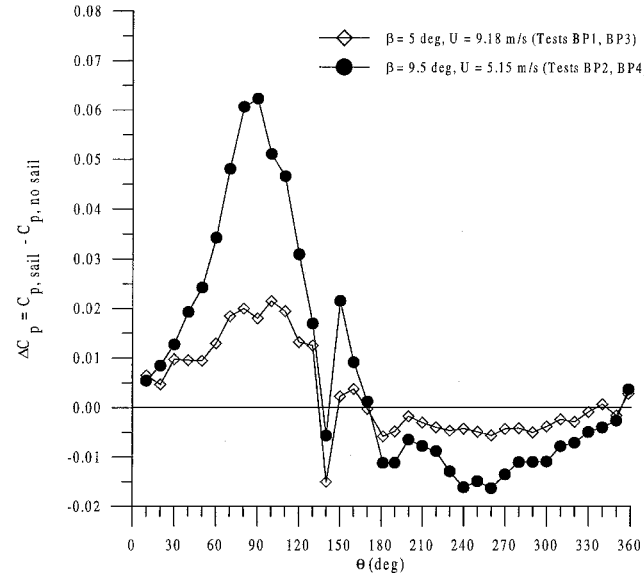

Fig. 12 Development of pressure difference with angle of drift: $x/L = 0.47$.

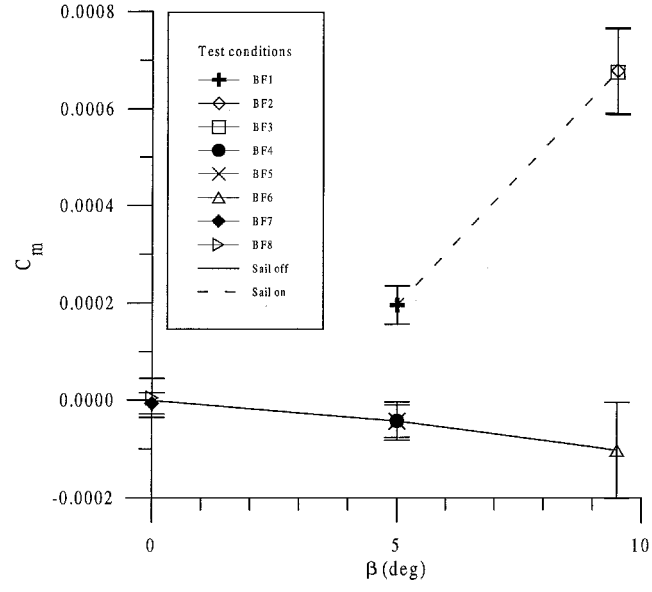

Fig. 13 Pitching moment variation with drift angle.

experiences due to the pressure variations. (By convention, a force directed from deck to keel corresponds to a positive value of C_Z.) Because these forces are located on the aft portion of the submarine, they yield the positive or nose-up pitching moment shown in Fig. 13.

Velocity Measurements

Two velocity components were measured, the streamwise component u parallel to the test section longitudinal axis and the transverse or vertical velocity component w perpendicular to the test section floor. Representative contour plots of these velocity components are shown in Figs. 15 and 16 for an angle of drift of 9.5 deg and an axial measurement position of $x/L = 0.47$. Figures 15 and 16 show true views of the measurement grid, that is, sighted along the axis of the submarine, and values of the streamwise and transverse velocity components. Recall that these grids were located as closely as possible to the same axial positions as the pressure tap rings. The highest level contour in Figs. 15 and 16 corresponds to the maximum value of the velocity component measured on that grid. Positive values are represented by solid lines and negative values by dashed lines. In Figs. 15 and 16, the jagged contour near the circle representing the model is the edge of the measurement grid closest to the model. In Figs. 15 and 16, the sail tip is located at the point

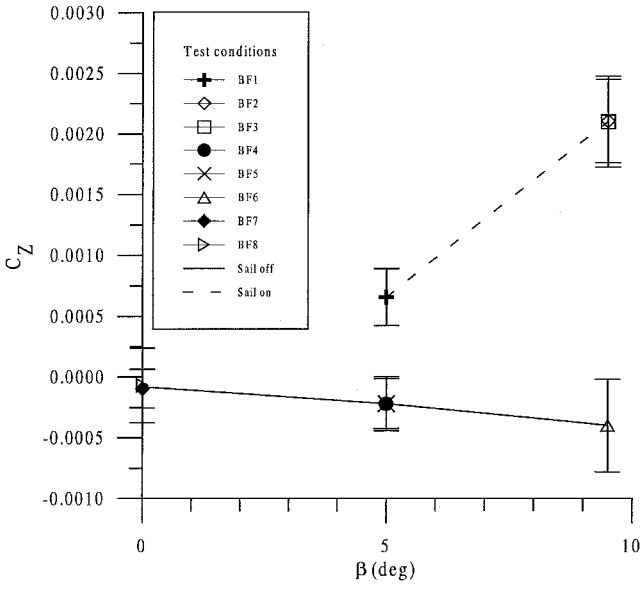

Fig. 14 Vertical force variation with drift angle.

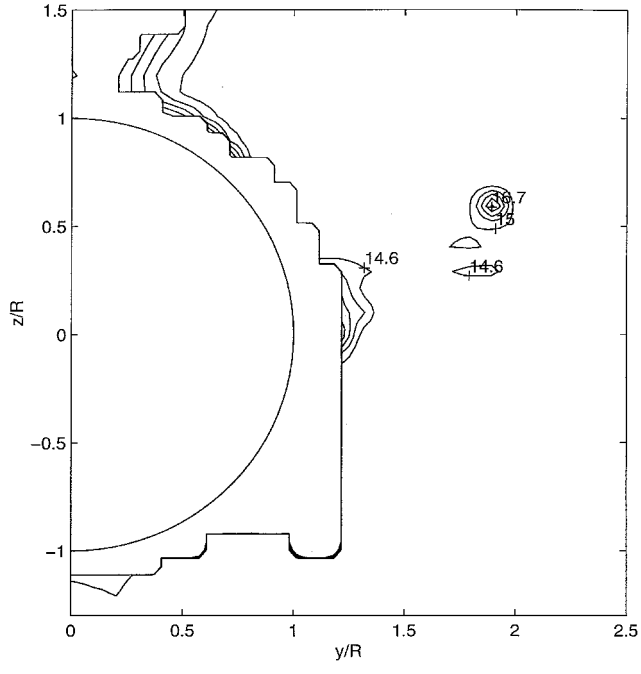

Fig. 15 Streamwise velocity component contours: $\beta = 9.5$ deg, $U = 14.8$ m/s, sail on, and $x/L = 0.47$ (test AV01). Maximum velocity value = 17.1 m/s; change in velocity value between contours = 0.43 m/s.

$(y/R, z/R) \approx (2, 0)$. For the data represented in Fig. 15, the maximum value of u measured was $u_{max} = 17.1$ m/s, over 15% higher than the freestream velocity of 14.8 m/s. The minimum contour level in Fig. 15 corresponds to $0.75u_{max}$, or 12.8 m/s. Figure 15 shows how tightly the tip vortex structure is organized. Because w is the vertical velocity component measured in the vicinity of the vortex, and because the vortex essentially aligns itself with the freestream direction, the results shown in Fig. 16 take on the appearance of a dipole distribution. The maximum absolute value of w measured on this grid was $w_{max} = 7.53$ m/s, or 51% of the freestream velocity. The resultant of the maximum values of u and w measured at this condition was $V_{max} = (u_{max}^2 + w_{max}^2)^{1/2} = 18.7$ m/s, yielding a maximum-velocity-to-freestream-velocity ratio $V_{max}/U = 1.26$.

The velocity measurements on which Figs. 15 and 16 are based were time averages and did not take into account vortex "meander." Also, the grids were somewhat sparse, to cover the flowfield in a reasonable amount of time. Therefore, it is likely that the maximum velocity measured was not necessarily the maximum velocity in

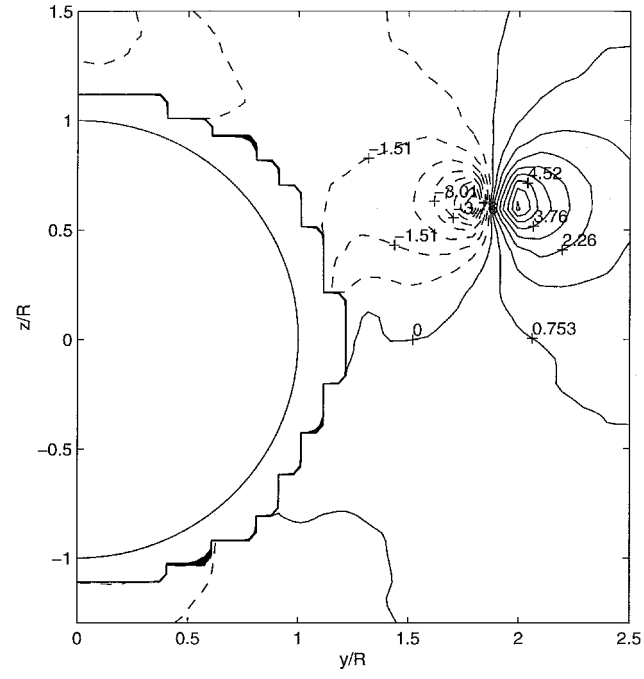

Fig. 16 Transverse (vertical or y) velocity component contours: $\beta = 9.5$ deg, $U = 14.9$ m/s, sail on, and $x/L = 0.47$ (test AV04). Maximum velocity value = 7.53 m/s; change in velocity value between contours = 0.75 m/s.

the flowfield. Thus, the apparent peaks shown by the contours in Figs. 15 and 16 do not necessarily indicate the precise positions of the vortex core.

Once the vortex core was located using the lower resolution grid, velocity surveys were made using a grid with a finer resolution, on which the grid spacing was reduced from $0.1R$ to $0.05R$, as already discussed. At the same drift angle of 9.5 deg and a freestream velocity of 14.8 m/s, the maximum value of the streamwise velocity found was $u_{max} = 17.6$ m/s, whereas the maximum value of transverse velocity found was $w_{max} = 11.25$ m/s, a substantial increase over the maximum transverse velocity found on the coarse grid. This increase was a result of values closer to the core being captured with the finer grid. The maximum resultant velocity was $V_{max} = 20.9$ m/s, yielding a velocity ratio $V_{max}/U = 1.41$. Although these maximal values do not quite approach the maximum ratio of 2.07 indicated by the results by Chow et al.,[22] they still demonstrate a substantial acceleration of the flow as a result of the formation of the tip vortex. The corresponding velocity values for the case $\beta = 5$ deg, $U = 9.33$ m/s, and $x/L = 0.47$ were $u_{max} = 9.45$ m/s, $w_{max} = 0.368$ m/s, and $V_{max}/U = 1.07$. These values were obtained using the fine-resolution grid. In terms of fractions of the freestream velocity, these values are smaller than the velocity maxima at $\beta = 9.5$ deg. This was to be expected because the vortex would not be as strong at the lower angle of attack for the sail.

The velocity data were used to obtain estimates of the vortex core position and circulation. Because the transverse velocity component v (the component perpendicular to the vertical walls of the tunnel test section) was not available, the usual circulation calculations, such as an integration around a contour containing the vortex, could not be performed. Therefore, to obtain at least an estimate of the circulation associated with the vortex, the following procedure was used. As will be seen shortly, the vortex shed from the tip of the sail aligned itself generally with the freestream velocity direction shortly after leaving the trailing edge of the sail. Therefore, in a vertical plane perpendicular to the freestream velocity, the flow resembled that induced by a point vortex. The expression for the velocity induced by such a vortex in a two-dimensional potential flow was used to compute the vertical velocity component induced at the point (y, z) by a point vortex located at (y_v, z_v):

$$w = \frac{\Gamma}{2\pi} \frac{y - y_v}{(y - y_v)^2 + (z - z_v)^2} \tag{5}$$

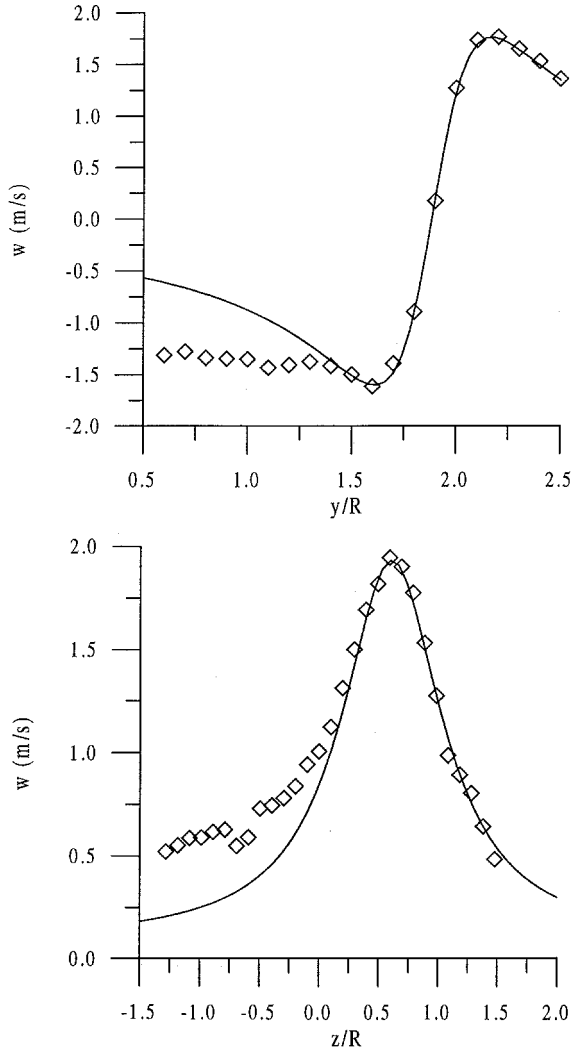

Fig. 17 Examples of curve fits to general vortex velocity function: $\beta = 9.5$ deg, $U = 14.9$ m/s, and $x/L = 0.47$.

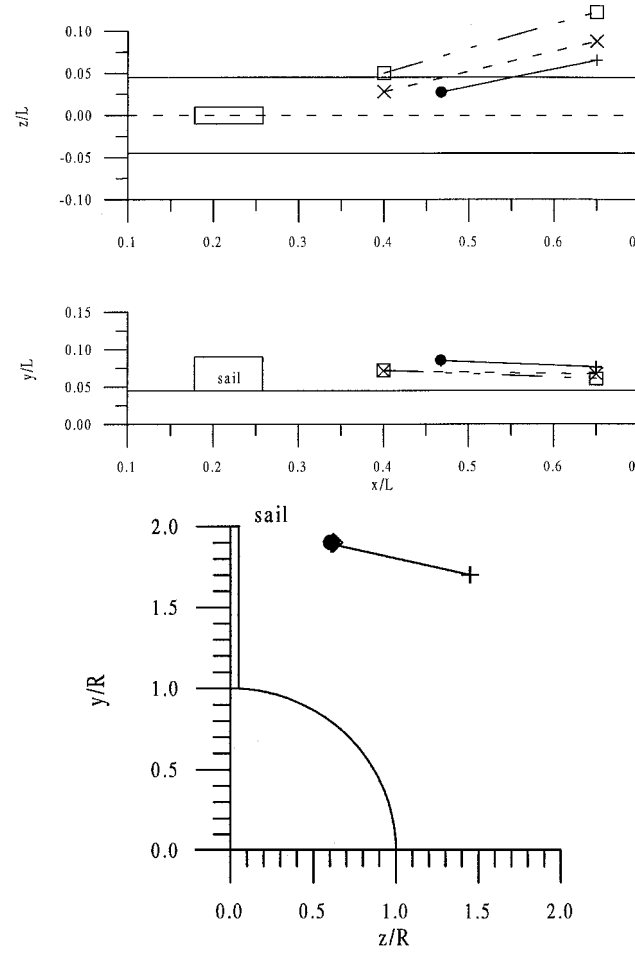

Fig. 18 Vortex trajectory data, $\beta = 9.5$ deg: +, $U = 14.9$ m/s (test AV04 and AV08); ◇, $U = 14.9$ m/s, detailed grid (test AV05); ●, $U = 7.64$ m/s (test AV03); ×, Liu and Fu[10] (rotating arm, 8-deg yaw); and □, Liu and Fu[10] (rotating arm, 16-deg yaw).

An iterative procedure was conducted to find values for Γ, y_v, and z_v that would produce a best-fit match between measured and computed values of w. Figure 17 is an example of the results, illustrating the w-velocity component values measured at particular y and z locations. The position of the vortex is obvious from the large variations of the velocity component. For y values inboard of the vortex, the flow is not approaching a zero velocity but a relatively constant negative velocity, caused by the downward deflection of the flow by the sail. It was evident from this sort of result that attempts to model the tip vortex as a potential vortex to determine the circulation would have to make use of data obtained only from outboard of the vortex position. The curvefits tended to be rather sensitive to the values of y_v, z_v, and particularly Γ, as one might expect when trying to fit data to a singular function. An uncertainty analysis was performed on the values of Γ so obtained. Typical values for the uncertainty in Γ were 16% at $\beta = 5$ deg and 11% at $\beta = 9.5$ deg. The uncertainties in the position coordinates y_v and z_v were assumed to be one-half the grid resolution, or $0.025R$.

The vortex trajectory data are shown in Fig. 18 for $\beta = 9.5$ deg. Included in Fig. 18 are vortex locations measured by Liu and Fu.[10] There were significant differences between the rotating-arm model used by Liu and Fu and the model in the current study, as well as the basic flow itself, but because the study by Liu and Fu is one of the few available in the open literature that examined many of the same flow phenomena that are being examined in the current study, it was decided that a comparison would be worthwhile to see if the flows were generally similar. Because the sail on the model used by Liu and Fu was located at a different x/L, their vortex locations were shifted by the difference in x/L values for the trailing edges of the sails. (The trailing edge of their sail was located at $x/L = 0.33$, whereas the trailing edge of the sail in the current study was located at $x/L = 0.26$.) The tops of the sails in both studies were located at $y/L \approx 0.045$, and so no vertical shift was added. No other changes were made to the values reported by Liu and Fu. Vortex trajectories from Liu and Fu for 8- and 16-deg yaw are shown. For an angle of yaw of 8 deg, the angle of attack at the sail varied between 0.843 deg at the leading edge and 3.67 deg at the trailing edge, with a value of 1.55 deg at the quarter chord of the sail. At a yaw angle of 16 deg, the angle of attack at the sail varied from 8.43 deg at the leading edge of the sail to 11.4 deg at the trailing edge, with a value of 9.18 deg at the quarter chord.

The data from both studies show that the tip vortex does in fact align itself generally with the freestream direction. For the current study, the angle between the vortex projection in the x–z plane and the x axis (the view in the top diagram of Fig. 18) is 11.8 deg. Recall the angle of attack of the sail is 9.5 deg. The total included angle between the vortex and the x axis is 12.1 deg. For the case of 8-deg yaw in the study by Liu and Fu, the angle between the vortex projection in the x–z plane and the x axis is 13.5 deg, and the total included angle is also 13.5 deg. For the case of 16-deg yaw, the angle between the vortex projection in the x–z plane and the x axis is 16.3 deg, and the total included angle is 16.5 deg. The current data seem to be consistent with the results of Liu and Fu in yielding angles that are slightly larger than the drift angle. In all cases, the vortex moves closer to the body in the x–z plane and to its image in the hull. This is consistent with the behavior of trailing vortices from aircraft wings.[23] Of course, the vorticity wrapped around the hull also has to be shed, and it is possible that this vorticity would interact with the control surfaces of the submarine.

Figure 19 compares the vortex trajectories for the two different angles of drift studied in the current experiments. For $\beta = 5$ deg, the

Table 5 Results of circulation estimates

Test	β, deg	U, m/s	x/L	γ	γ_{cv}	γ_{wing}	γ_{Wald}
AV04	9.5	14.9	0.47	0.018	1.2	0.0121	0.0165
AV05	9.5	14.9	0.47	0.018	1.2	0.0121	0.0165
AV03	9.5	7.64	0.47	0.018	1.2	0.0121	0.0165
AV08	9.5	14.9	0.65	0.019	1.3	0.0121	0.0165
BV02	5	9.29	0.468	0.0065	0.84	0.0063	0.00868
BV04	5	9.39	0.468	0.0066	0.83	0.0063	0.00868
BV06	5	9.39	0.585	0.0071	0.9	0.0063	0.00868
BV08	9.5	5.23	0.475	0.017	1.1	0.0121	0.0165
BV10	9.5	5.24	0.475	0.017	1.2	0.0121	0.0165
BV14	9.5	5.28	0.618	0.017	1.1	0.0121	0.0165

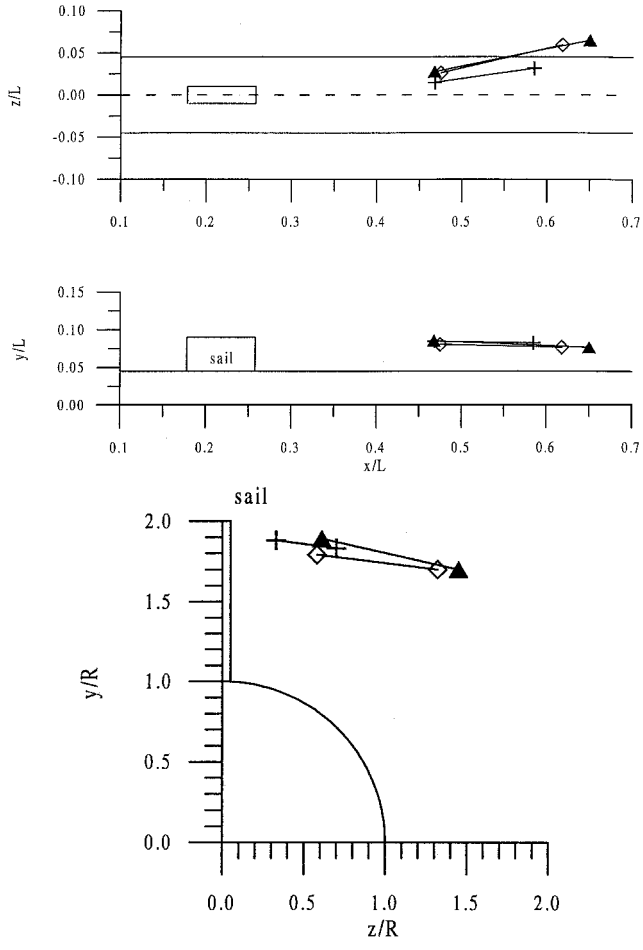

Fig. 19 Comparison of vortex trajectory data at both angles of drift: +, $\beta = 5$ deg (phase 2, tests BV04 and BV06); ▲, $\beta = 9.5$ deg (phase 1, tests BV04 and BV08); and ◇, $\beta = 9.5$ deg (phase 2, tests BV10 and BV14).

angle between the vortex projection in the x–z plane and the x axis was 8.11 deg, and the total included angle was 8.13 deg. Figure 19 also compares the measurements of the trajectories measured at $\beta = 9.5$ for both test phases. The projection angle in the second phase was 13.1 deg, and the total included angle was 13.2 deg. These are slightly higher than the values obtained during the first test phase. However, there is otherwise relatively good agreement in the vortex trajectories between the two test phases.

The results for the circulation values are listed in Table 5. The dimensionless circulation values γ and γ_{cv} are defined in the following manner:

$$\gamma = \Gamma/UL, \qquad \gamma_{cv} = \Gamma/U \sin\beta D \tag{6}$$

where L is the model length and D is the model diameter. The first definition is the standard definition, whereas the second defines the dimensionless variable in terms of the crossflow velocity component $U \sin\beta$ and the model diameter D.

In addition to the values estimated from the velocity measurements, Table 5 also includes values predicted by two different versions of finite wing theory. By using the Kutta–Joukowski theorem, the circulation γ as defined in Eq. (6) may be related to the angle of drift according to the following formula:

$$\gamma = \tfrac{1}{2}(c/L)a\beta \tag{7}$$

In Eq. (7), c is the sail chord length and a is the lift-curve slope of the finite wing. According to Jones,[24] the lift-curve slope for a low-aspect-ratio wing is given by

$$a = \pi AR_s, \qquad AR_s = h/c \tag{8}$$

Here, the simple definition of the sail aspect ratio as the ratio of the sail height above the deck h to the sail chord c has been used. In the context of finite wing theory, this would be half the usual aspect ratio value because the sail would actually form only half of the finite wing. Wald[25] used a Trefftz-plane analysis from potential flow theory to examine the flow downstream of a slender body with a single fin to determine the lift force on the fin itself and on the body. His result for the lift-curve slope for the fin was

$$a = \pi AR_s J_1 \tag{9}$$

where J_1 is given by

$$J_1 = (4/\pi)(R/h)^2\left\{\tfrac{1}{2}(t+1)^2\left[\pi/2 + \sin^{-1}\sqrt{(t-1)/(t+1)}\right] - \pi - (3-t)\sqrt{\tfrac{1}{2}(t-1)}\right\}$$

$$t = \tfrac{1}{2}[(R+h)/R + R/(R+h)] \tag{10}$$

In Fig. 20, the results for the circulation estimates in the current experiment are compared to the theoretical predictions and to values determined by Liu and Fu[10] from measurements of the wake of the sail. With both in-plane velocity components available, Liu and Fu were able to perform a standard contour integration to obtain the circulation associated with the sail tip vortex. In Fig. 20, the correct values of the angle of attack at the quarter-chord of the sail reported by Liu and Fu are used as the drift angles β. (The values shown on p. 12 of Ref. 10 are actually the angles of attack at the $0.75c$ location.) Also included in Fig. 20 for purposes of comparison are

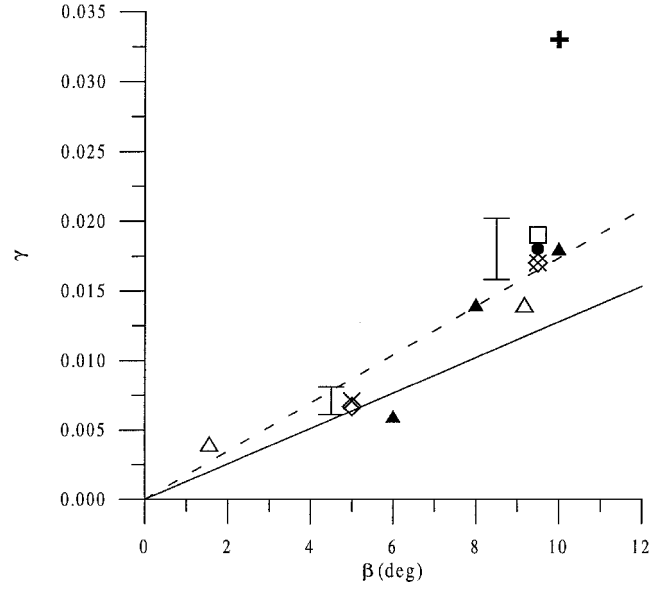

Fig. 20 Comparison of estimated circulation values with theories and with other measurements; indications of typical uncertainties in the current measurements at $\beta = 5$ deg and $\beta = 9.5$ deg shown: ●, $x/L = 0.47$ (tests AV04, AV05, and AV03); □, $x/L = 0.65$ (tests AV08); ◇, $x/L = 0.47$ (tests BV02 and BV08); ×, $x/L = 0.62$ (tests BV14); △, Liu and Fu[10]; ▲, Rokhsaz et al.,[27] flat plate; +, Desabrais and Johari,[26] NACA 0012; ——, finite wing theory, Jones[24]; and – – –, theory by Wald.[25]

measurements of the circulation of tip vortices generated by half-wings extending from the wall of a wind or water tunnel, that is, no centerbody or fuselage. The results from Desabrais and Johari[26] are for a flat plate with a semispan aspect ratio of 1.5, and the results from Rokhsaz et al.[27] are for a wing with an NACA 0012 airfoil section and a semispan aspect ratio of 2.1. The half-wing results have been multiplied by the ratio of the sail chord to the overall hull length for inclusion in Fig. 20.

As can be seen in Table 5, the results for the current circulation estimates were quite consistent with one another. For $\beta = 9.5$ deg in the first test phase, the circulations measured using the coarse and fine grids differed only slightly at $x/L = 0.47$, and the circulation measured at the downstream position $x/L = 0.65$ was only slightly larger than the upstream value. The measurements made at two different speeds confirmed the dependence of the dimensionless circulation on the drift angle only. For $\beta = 9.5$ deg in the second test phase, the estimated values were only slightly less than the values from the first test phase, and the downstream value was in fact equal to the upstream value, indicating a constant circulation associated with the tip vortex. For $\beta = 5$ deg in the second test phase, the values were also consistent, with the downstream value showing a slightly larger increase. In general there seems to be a fair amount of scatter among the different experiments, with the theory by Wald[25] predicting the results most closely.

The circulation associated with the sail tip vortex may be used along with airfoil theory in one final calculation. If we assume that the circulation in the vortex is equivalent to the circulation around the sail (thought of now as an airfoil at angle of attack), then we may also assume that an equivalent amount of circulation exists around the submarine hull. Coney[28] made measurements of the circulation along a contour around the sail mounted at angle of attack on a submarine hull and of the circulation around the submarine hull and found that the ratio of the two values of the circulation was very close to one. As a result of this, we can think of the vorticity attached to the submarine as something akin to a classical horseshoe vortex, where the base of the horseshoe is bound to the sail, one leg is the sail tip vortex, and the other is actually enlarged and wrapped around the submarine hull. It is this argument that allows us to equate the circulation in the tip vortex with the circulation bound to the sail and, thus, the circulation around the submarine hull.

It is then possible to use the Kutta–Joukowski theorem along with the circulation around the hull and the crossflow velocity component to compute the vertical force per unit length acting on the hull that contributes to the pitching moment:

$$F_z = \rho(U \sin\beta)\Gamma \Rightarrow c_z = \frac{F_z}{\frac{1}{2}\rho U^2 R}$$

$$= \frac{\rho(U \sin\beta)(UL\gamma)}{\frac{1}{2}\rho U^2 (D/2)} = 4\left(\frac{L}{D}\right)\gamma \sin\beta \tag{11a}$$

This equation may also be written in terms of the dimensionless crossflow circulation γ_{cv}:

$$F_z = \rho(U \sin\beta)\Gamma \Rightarrow c_z = \frac{F_z}{\frac{1}{2}\rho U^2 R}$$

$$= \frac{\rho(U \sin\beta)(U \sin\beta D\gamma_{cv})}{\frac{1}{2}\rho U^2 (D/2)} = 4\gamma_{cv} \sin^2\beta \tag{11b}$$

For small angles, $\sin\beta \approx \beta$ and so $c_z \approx 4\gamma_{cv}\beta^2$, illustrating the dependence of the vertical force coefficient on the square of the drift angle, as discussed earlier. The results of these computations are compared in Table 6 to the results of the pressure integrations discussed earlier. In Table 6, the values of c_z computed using Eq. (11b) with the circulation estimates obtained using Eq. (5) are denoted by $c_{z,\text{exp}}$. The sectional side force coefficients computed using the low-aspect-ratio finite-wing theory of Jones,[24] represented by Eq. (8), and the theory by Wald,[25] represented by Eq. (9), are denoted by $c_{z,\text{wing}}$ and $c_{z,\text{Wald}}$, respectively. For these two computations, the lift curve slopes given by Eqs. (8) and (9) are used in Eq. (7) to compute the dimensionless circulation γ, which is then used in Eq. (11a) to compute the sectional side force coefficient. Note that for a given drift angle β these calculated values will not change with freestream velocity. The values are repeated in Table 6 merely for convenience. The last column contains the corresponding values of the sectional side force coefficient obtained by integrating the measured pressure distributions using Eq. (4). These values are denoted by $c_{z\,\text{int}}$. Recall that these values were obtained by taking the difference in the pressure coefficient values with the sail on and the sail off and integrating that difference, so that each integration was actually the result of two separate runs. Because a number of pressure taps from the downstream tap ring had to be omitted in phase 2, no pressure integrations were computed at this location in phase 2. These conditions are denoted by an x in Table 6.

Table 6 Comparisons of sectional force calculations

Phase	β, deg	x/L	U, m/s	$c_{z,\text{exp}}$	$c_{z,\text{wing}}$	$c_{z,\text{Wald}}$	$c_{z,\text{int}}$
1	9.5	0.47	14.9	0.13	0.0889	0.121	0.096
1	9.5	0.47	14.9	0.13	0.0889	0.121	——
1	9.5	0.47	7.64	0.13	0.0889	0.121	0.088
1	9.5	0.65	14.9	0.14	0.0889	0.121	0.090
2	5	0.468	9.29	0.026	0.0247	0.0336	0.032
2	5	0.468	9.39	0.025	0.0247	0.0336	——
2	5	0.585	9.39	0.027	0.0247	0.0336	x
2	9.5	0.475	5.23	0.12	0.0889	0.121	0.088
2	9.5	0.475	5.24	0.13	0.0889	0.121	——
2	9.5	0.618	5.28	0.12	0.0889	0.121	x

At the higher angle of drift, $\beta = 9.5$ deg, the values of $c_{z,\text{exp}}$ agree closely with the values predicted by the theory of Wald[25] ($c_{z,\text{Wald}}$), as might have been expected, because the circulation values also agreed closely. The agreement is slightly better in the phase 2 results. Note, however, that at $\beta = 9.5$ deg, the low-aspect-ratio finite-wing predictions $c_{z,\text{wing}}$ agree fairly well with the values obtained by integrating the pressure distributions, $c_{z,\text{int}}$. This agreement is consistent between the two phases. At the lower angle of drift, $\beta = 5$ deg, the values of $c_{z,\text{exp}}$ agree closely to the values of $c_{z,\text{wing}}$, again a result that might have been expected, because the circulation values also agreed relatively closely at $\beta = 5$ deg. Note in this case, however, that the pressure integration values $c_{z,\text{int}}$ are in closer agreement with $c_{z,\text{Wald}}$ than they are with $c_{z,\text{wing}}$. At $\beta = 9.5$ deg, the values of the circulation obtained from the measured velocity fields were usually larger than the values measured by other investigators and the values obtained from the most common theory (the low-aspect-ratio finite-wing theory by Jones[24]). These values led to values of $c_{z\,\text{exp}}$ that exceeded $c_{z,\text{wing}}$. The agreement between $c_{z,\text{wing}}$ and $c_{z,\text{int}}$ at $\beta = 9.5$ deg suggests that the values of $c_{z,\text{exp}}$ were possibly being overpredicted. The reasons then for the almost complete reversal of the situation at $\beta = 5$ deg, where $c_{z,\text{exp}}$ is in fairly good agreement with $c_{z,\text{wing}}$ and $c_{z,\text{int}}$ is in relatively close agreement with $c_{z,\text{Wald}}$ are unknown. It is quite possible that in this case it is $c_{z,\text{int}}$ that is most in error. The pressure distributions at the lower value of β were less well defined, and this combined with the large spacing between the pressure taps could have increased the error in the integration.

Conclusions

The pressure distributions measured in these tests are consistent with the mechanism postulated by Feldman[3] and others by which the tip vortex shed from the sail at angle of drift during a high-speed turn causes an out-of-plane moment, in particular a pitching moment: The circulation associated with the vortex creates an equal and opposite circulation about the hull that results in a shift in the pressure distribution, increasing the pressure on the deck of the hull and decreasing the pressure on the keel. Because this net downward force acts primarily on the rear of the submarine, the net result is a nose-up pitching moment. The forces and moments measured in these tests were also in agreement with this theory.

The velocity field measurements demonstrated that the axial and tangential velocity components in the vortex core could reach very large values. The axial velocity component in some cases exceeds the freestream value by 40%, and the maximum tangential velocity component was sometimes as large as the freestream velocity. The vortices generally aligned themselves with the freestream velocity direction, usually making an angle that was greater than the drift angle by 1 or 2 deg.

Estimates of the circulation associated with the tip vortex were in general agreement with those measured by other investigators and with values predicted by finite-wing and potential flow theory. Estimates of the vertical force section coefficient obtained from the estimated circulation values were in general agreement with values obtained by integrating the measured pressure distributions. Both the vertical force section coefficients obtained from integrating the pressure distributions and the vertical force coefficients obtained by measuring the forces on the model exhibited the nonlinear variation with angle of drift predicted by the theories.

Over the range of Reynolds numbers at which tests were conducted in this investigation, the results showed very little dependence on Reynolds number. Doubling the Reynolds number had very little effect on either pressure distributions or velocity field measurements.

Acknowledgments

This work was supported by Office of Naval Research Grant N00014-96-1-0911, L. Patrick Purtell, Monitor, under the Defense Experimental Program to Stimulate Competitive Research. Additional support was provided to the first author by the Department of Aerospace Engineering, Mississippi State University, John C. McWhorter III, Head. The authors gratefully acknowledge the financial support for this study. Robert Etter of the Naval Surface Warfare Center, Carderock Division, provided significant assistance during the planning stages of this study, and his help is also gratefully acknowledged. The assistance of Keith Koenig, Professor of Aerospace Engineering, Mississippi State University, in the revision process is gratefully acknowledged.

References

[1]Gruner, W. P., and Payne, H. E., III, "Submarine Maneuver Control," *Proceedings*, U.S. Naval Inst., Vol. 118, No. 7, Annapolis, MD, 1992, pp. 56–60.

[2]Wright, J. E., "Submarine Design for the Littorals," *Proceedings*, U.S. Naval Inst., Vol. 121, No. 12, Annapolis, MD, 1995, pp. 39–41.

[3]Feldman, J. P., "Method of Performing Captive-Model Experiments to Predict the Stability and Control Characteristics of Submarines," Carderock Div., Rept. CRDKNSWC-HD-0393-25, U.S. Naval Surface Warfare Center, Bethesda, MD, June 1995.

[4]Groves, N., Huang, T., and Chang, M., "Geometric Characteristics of DARPA SUBOFF Models," David Taylor Research Center, Rept. SHD-1298-01, Bethesda, MD, March 1989.

[5]Roddy, R. F., "Investigation of the Stability and Control Characteristics of Several Configurations of the DARPA SUBOFF Model (DTRC Model 5470) from Captive-Model Experiments," David Taylor Research Center, Rept. DTRC/SHD-1298-08, Bethesda, MD, Sept. 1990.

[6]Jonnalagadda, R., "Reynolds-Averaged Navier–Stokes Computation of Forces and Moments for Appended SUBOFF Configurations at Incidence," M.S. Thesis, Computational Engineering Dept., Mississippi State Univ., Mississippi State, MS, May 1996.

[7]Jonnalagadda, R., Taylor, L., and Whitfield, D., "Multiblock Multigrid Incompressible RANS Computation of Forces and Moments on Appended SUBOFF Configurations at Incidence," AIAA Paper 97-0624, 1997.

[8]Zierke, W. (ed.), "A Physics-Based Means of Computing the Flow Around a Maneuvering Underwater Vehicle," Applied Research Lab., TR 97-0002, Pennsylvania State Univ., University Park, PA, Jan. 1997.

[9]Sung, C., Fu, T., Griffin, M., and Huang, T., "Validation of Incompressible Flow Computation of Forces and Moments on Axisymmetric Bodies Undergoing Constant Radius Turning," *Twenty-First Symposium on Naval Hydrodynamics*, National Academy Press, Washington, DC, 1997, pp. 1061–1076.

[10]Liu, H., and Fu, T., "PDV Measurement of Vortical Structures in the DTMB Rotating Arm Facility," Carderock Div., Rept. CRDKNSWC/HD-1416-02, U.S. Naval Surface Warfare Center, Bethesda, MD, Sept. 1994.

[11]Liu, H., Beglin, G., and Fu, T., "Implementation of PDV Technology in the Rotating Arm Facility," Carderock Div., CRDKNSWC/HD-1416-01, U.S. Naval Surface Warfare Center, Bethesda, MD, March 1993.

[12]Wetzel, T., Simpson, R., and Liapis, S., "The Effects of Vortex Generating Fins and Jets on the Crossflow Separation of a Submarine in a Turning Maneuver," Dept. of Aerospace and Ocean Engineering, Rept. VPI-AOE-195, Virginia Polytechnic Inst. and State Univ., Blacksburg, VA, May 1993.

[13]Wetzel, T., and Simpson, R., "Effects of Fin and Jet Vortex Generators on the Crossflow," *Journal of Aircraft*, Vol. 35, No. 3, 1998, pp. 370–379.

[14]Etter, R., and Wilson, M., "The Large Cavitation Channel," *Proceedings of the 23rd American Towing Tank Conference*, Univ. of New Orleans, New Orleans, LA, 1992, pp. 243–252.

[15]Etter, R., and Wilson, M., "Testing Ship Designs in a Water Tunnel," *Mechanical Engineering*, Vol. 13, No. 10, 1993, pp. 74–80.

[16]Blanton, J., "Laser Doppler Velocimetry Techniques in the Large Cavitation Channel," *Proceedings of the 24th American Towing Tank Conference*, Offshore Technology Research Center, Texas A&M Univ., College Station, TX, 1995, pp. 95–102.

[17]Blanton, J., and Etter, R., "Laser Doppler Velocimetry on a Body of Revolution in the Large Cavitation Channel," *Laser Anemometry—1995*, FED Vol. 229, edited by T. T. Huang, J. Turner, M. Kawahashi, and M. V. Otugen, American Society of Mechanical Engineers, New York, 1995, pp. 379–385.

[18]Blanton, J., "Uncertainty Estimates of Test Section Pressure and Velocity in the Large Cavitation Channel," AIAA Paper 95-3079, July 1995.

[19]Coleman, H., and Steele, W., *Experimentation and Uncertainty Analysis for Engineers*, Wiley, New York, 1989, pp. 35–37, 77–100.

[20]Coleman, H., and Steele, W., *Experimentation and Uncertainty Analysis for Engineers*, 2nd ed., Wiley, New York, 1999, pp. 38–43, 85–112.

[21]Bridges, D. H., "A Detailed Study of the Flow Field of a Submarine at Large Angle of Drift," Dept. of Aerospace Engineering, Rept. MSSU-ASE-01-1, Mississippi State Univ., Mississippi State, MS, May 2001.

[22]Chow, J., Zilliac, G., and Bradshaw, P., "Mean and Turbulence Measurements in the Near Field of a Wingtip Vortex," *AIAA Journal*, Vol. 35, No. 10, 1997, pp. 1561–1567.

[23]Pope, A., *Basic Wing and Airfoil Theory*, McGraw–Hill, New York, 1951, pp. 227–229.

[24]Jones, R. T., "Properties of Low-Aspect-Ratio Pointed Wings at Speeds Below and Above the Speed of Sound," NACA Rept. 835, March 1946.

[25]Wald, Q., "The Hydrodynamic Forces on Fin–Body Combinations," Electric Boat Div., Rept. P-411-67-077, General Dynamics Corp., Groton, CT, Dec. 1967.

[26]Desabrais, K. J., and Johari, H., "Direct Circulation Measurement of a Tip Vortex," *AIAA Journal*, Vol. 38, No. 11, 2000, pp. 2189–2191.

[27]Rokhsaz, K., Foster, S. R., and Miller, L. S., "Exploratory Study of Aircraft Wake Vortex Filaments in a Water Tunnel," *Journal of Aircraft*, Vol. 37, No. 6, 2000, pp. 1022–1027.

[28]Coney, W. B., "Circulation Measurements About a Body of Revolution with an Attached Fin," M.S. Thesis, Dept. of Ocean Engineering, Massachusetts Inst. of Technology, Cambridge, MA, June 1985.

P. R. Bandyopadhyay
Associate Editor